Heteroleptic iron(II) spin crossover complexes based on a 2,6-bis(pyrazol-1-yl)pyridine-type ligand functionalized with a carboxylic acid

Víctor García-López,[a] *Mario Palacios-Corella,*[a] *Verónica Gironés-Pérez,*[a] *Carlos Bartual-Murgui,* [a]* *José Antonio Real,* [a] *Eric Pellegrin,*[b] *Javier Herrero-Martín,*[b] *Guillem Aromí,*[c]*
Miguel Clemente-León [a]* *and Eugenio Coronado* [a]

[a] Instituto de Ciencia Molecular (ICMol), Universidad de Valencia, Catedrático José Beltrán 2,
46980 Paterna, Spain

[b] ALBA Synchrotron Light Source, 08290 Cerdanyola del Vallès, Barcelona, Spain

[c] Departament de Química Inorgànica i Orgànica, Universitat de Barcelona and Institute of
Nanoscience and Nanotechnology (IN2UB), Diagonal 645, 08028 Barcelona, Spain.

ABSTRACT. Two new heteroleptic complexes $[Fe(1bppCOOH)(3bpp\text{-}bph)](ClO_4)_2\cdot solv$ (**1·solv**, solv = various solvents; 1bppCOOH = 2,6-bis(1H-pyrazol-1-yl)isonicotinic acid; 3bpp-bph = 2,6-bis(5-([1,1'-biphenyl]-4-yl)-1H-pyrazol-3-yl)pyridine) and $[Fe(1bppCOOH)(1bppCOOEt)](ClO_4)_2\cdot 0.5Me_2CO$ (**2·0.5Me$_2$CO**, 1bppCOOEt = ethyl 2,6-bis(1H-pyrazol-1-yl)isonicotinate) have been designed and prepared. The heteroleptic compound **1·solv** was obtained by the combination of stoichiometric amounts of $Fe(ClO_4)_2$, 1bppCOOH and 3bpp-bph, and it was designed to fine tune the spin crossover (SCO) properties with respect to the previously reported homoleptic compound $[Fe(1bppCOOH)_2](ClO_4)_2$. Indeed, the introduction of a new substituted 3bpp ligand induces a weaker ligand field in addition to promoting the formation of π···π and C−H···π intermolecular interactions through the biphenyl groups. For the desolvated counterpart **1**, this results into a shift of the SCO curve towards room temperature and the observation of a 13 K hysteresis width. Besides, compound **2·0.5Me$_2$CO**, which represents the first example of a heteroleptic complex containing two 1bpp tridentate ligands, stabilizes the LS state at room temperature confirming the same trend observed for the corresponding homoleptic compounds. Interestingly, both **1** and **2·0.5Me$_2$CO** heteroleptic complexes exhibit photo-switchable properties when irradiating with a 523 nm laser at 10 K. Preliminary characterization of the deposited complexes on native SiO_2 by X-Ray Absorption **(**XAS) measurements suggests oxidation and decomposition of the complexes.

Introduction

Spin-crossover (SCO) complexes can be reversibly switched between two distinct states by a variety of external inputs such as light, temperature, pressure, analytes or electric fields.[1,2] The most appealing case is that of Fe(II), which switches between the diamagnetic low-spin state (LS, S = 0) and the paramagnetic high-spin state (HS, S = 2) while undergoing changes of the metal-to-donor atom bond distances and of the optical and dielectric properties. Thus, since the SCO phenomenon induces reversible changes of a number of physical properties, these materials constitute an ideal and promising platform for many applications such as sensors, memories or as part of spintronic devices.[3]

Bis-chelated iron(II) complexes based on tridentate ligands of the type 2,6-bis(pyrazol-x-yl)pyridine (x = 1 or 3, i.e., 1bpp[4–8] or 3bpp[9]) are very attractive, since they generate the appropriate ligand field to observe the SCO phenomenon in the Fe(II) ion and lead to complexes with a dense network of intermolecular interactions affecting in very interesting ways the dynamics of the magnetic transition. Hence, these complexes usually present abrupt thermal spin transitions at accessible temperatures and the Light-Induced Excited Spin State Trapping (LIESST) effect.[10,11] In addition, the spin state of these systems is known to be very sensitive to solvent exchange through the molecular network[9,12–14] and, consequently, they can act as chemo-responsive materials. We recently discovered that the mixture of an iron(II) salt with two different 3bpp ligands of varying length led to the quantitative crystallization of the heteroleptic complex out of all the possible combinations of two ligands per metal.[15] Later on, we expanded this investigation to other 3bpp derivatives in combination with the 2,6-bis(pyridin-2-yl)pyridine (tpy) and the 2,6-bis(benzimidazol-2-yl)pyridine (2bbp) ligands,[16] confirming a marked tendency of the Fe(II) ion to form heteroleptic $[Fe(L)(L')](ClO_4)_2$ complexes from pairs of chelating tris-imine ligands. This quasi-exclusive formation of heteroleptic adducts has been proven as a prolific source of new compounds with very diverse properties.[17,18]

In previous reports, we showed that the solvent-free perchlorate salt of the homoleptic iron(II) complex of the ligand 1bppCOOH (2,6-di(1H-pyrazol-1-yl)isonicotinic acid, Scheme 1) exhibits a hysteretic (3 K) abrupt thermal spin transition at high temperatures (380 K) affected by the presence of a linear network of hydrogen-bonded complexes.[19] Moreover, it has been proved that the introduction of a carboxylic acid group on the 4-pyridyl position promotes the formation of a polynuclear metal complex[20] and could facilitate the anchoring to metal-oxide surfaces. Besides, the homoleptic complex formed by the related 1bppCOOEt ligand (ethyl-2,6-di(1H-pyrazol-1-yl)isonicotinate) presents two solvates: $[Fe(1bppCOOEt)_2](ClO_4)_2{\cdot}0.75Me_2CO$ shows an abrupt LS-to-HS solvent-induced SCO around 330 K that becomes irreversible once the complex loses the solvent molecules remaining in the HS state;[21] $[Fe(1bppCOOEt)_2](ClO_4)_2{\cdot}MeCN$ exhibits solvent-dependent thermal SCO in the temperature range 180-290 K with a thermal hysteresis ca. 100 K wide, for the first cooling and heating cycle.[22]

In this work, we intend to take advantage of the properties of ligand 1bppCOOH while incorporating additional features to its SCO materials by extending the family of its iron(II) complexes to heteroleptic species. We have thus combined it with ligands 3bpp-bph (2,6-bis(5-([1,1'-biphenyl]-4-yl)-1H-pyrazol-3-yl)pyridine) or 1bppCOOEt (Scheme 1) yielding, respectively, the corresponding heteroleptic complexes $[Fe(1bppCOOH)(3bpp\text{-}bph)](ClO_4)_2{\cdot}solv$ (**1·solv**, solv = various solvents) and $[Fe(1bppCOOH)(1bppCOOEt)](ClO_4)_2{\cdot}0.5Me_2CO$ (**2·0.5Me$_2$CO**). In compound **1·solv**, the 3bpp-bph ligand has been selected with two main goals: i) decreasing the SCO temperature with respect to the homoleptic $[Fe(1bppCOOH)_2](ClO_4)_2$ counterpart by exploiting a ligand with a potentially weaker crystal field; ii) increasing the number of π···π and C−H···π interactions through the biphenyl groups in order to improve the connectivity between Fe(II) centers and, therefore, the cooperativity of the system. Concerning compound **2·0.5Me$_2$CO**, it represents, to the best of our knowledge, the first example of a heteroleptic complex formed by two 1bpp-type ligands. On the other hand, these two complexes are suitable for anchoring on metal-oxide surfaces thanks to the presence of a grafting ligand (bppCOOH), while the second ligand, in the case of **1**, could favor π···π and C−H···π interactions among the deposited complexes on the surface. The spin-crossover properties, structural characterization and LIESST effect behaviors of **1·solv**, **2·0.5Me$_2$CO** and their desorbed counterparts are discussed here together with a preliminary characterization of their deposition.

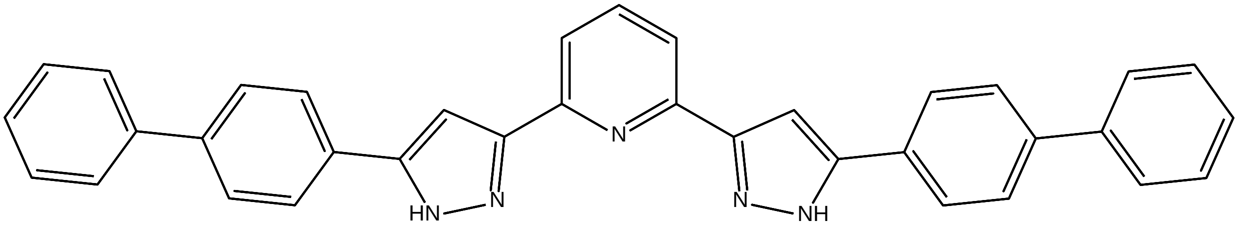

3bpp-bph

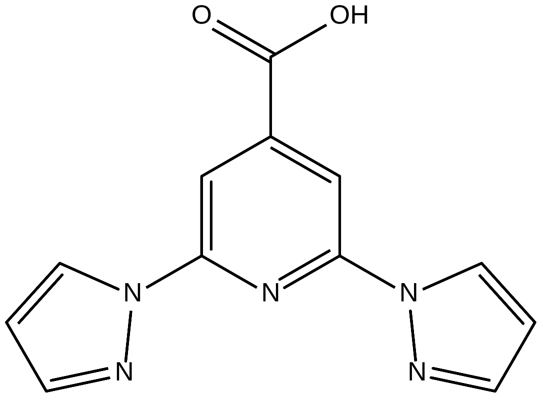

1bppCOOH

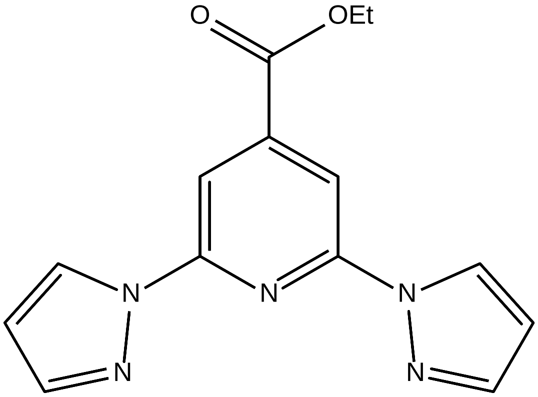

1bppCOOEt

Scheme 1. Representation of the ligands used in this work.

Experimental section

1bppCOOH[19] and 1bppCOOEt[23] were prepared according to literature methods. All other chemicals are commercially available and were used as received without further purification.

Synthesis

3bpp-bph. The synthesis of 3bpp-bph was carried out in two steps.

Step I: Synthesis of the precursor 2,6-bis-(1-([1,1'-biphenyl]-4-yl)-3-oxopropanoyl)-pyridine (**3bpp-bph-prec**). A 60% oil dispersion of NaH (2.09 g, 52.2 mmol) was washed for 20 min under N_2 with hexane. The solvent was extracted using a filter cannula, and tetrahydrofuran (THF, 25 mL) was added. Then, 1-([1,1'-biphenyl]-4-yl)ethan-1-one (1.77 g, 9.03 mmol) and dimethyl-2,6-pyridinedicarboxylate (1.01 g, 4.5 mmol) were dissolved in THF (25 mL) under a nitrogen atmosphere. This mixture was added dropwise with stirring over the NaH suspension. After the addition was completed, the reaction mixture was heated to reflux, turning from yellow to orange after a few hours, and left overnight. The mixture was then left to cool to room temperature, and some drops of EtOH were added in order to quench any remaining NaH, followed by careful addition of 100 mL of water. HCl 37% (20 mL) was then added changing the pH from 14 to 3 that resulted in the precipitation of a light-yellow solid which was filtered, washed with diethyl ether and dried in air. The yield was 1.2 g (44%). ^1H NMR (400 MHz, ppm in $CDCl_3$): 8.25 (d, 2H), 8.15-8.05 (m, 4H), 8.05-7.95 (m, 1H), 7.76-7.65 (m, 6H), 7.63-7.55 (m, 2H), 7.47-7.32 (m, 6H), 2.30 (s, 2H), 1.8 (s, 2H).

Preparation of 2,6-bis-(5-([1,1'-biphenyl]-4-yl)-1H-pyrazol-3-yl)-pyridine (3bpp-bph). Solid **3bpp-bph-prec** (0.45 g, 0.86 mmol) was refluxed overnight with hydrazine monohydrate (0.27

g, 8.6 mmol) in MeOH (40 mL). After cooling to room temperature, the off-white suspension was filtered and washed with diethyl ether giving place to a white precipitate which was dried in air. The yield was 0.41 g (92%). ^{1}H NMR (400 MHz, ppm in DMSO-d6): 13.60 (broad s, 2H), 8.20-7.90 (broad m, 5H), 7.90-7.70 (broad m, 9H), 7.65-7.42 (broad m, 6H), 7.45-7.25 (m, 3H).

Synthesis of [[Fe(1bppCOOH)(3bpp-bph)]$(ClO_4)_2$·2Me_2CO·0.5Et_2O (1·2Me_2CO·0.5Et_2O), [Fe(1bppCOOH)(3bpp-bph)]$(ClO_4)_2$·Me_2CO (1·Me_2CO) and [Fe(1bppCOOH)(1bppCOOEt)]$(ClO_4)_2$·0.5Me_2CO (2·0.5Me_2CO)

CAUTION: perchlorate salts are explosive when heated or subjected to friction.

A solution of $Fe(ClO_4)_2·xH_2O$ (7.64 mg, 0.03 mmol) in acetone (1.5 mL) was added to a solution of 1bppCOOH (7.68 mg, 0.03 mmol) and 3bpp-bph (15.42 mg, 0.03 mmol) in acetone (1.5 mL) or 1bppCOOH (7.68 mg, 0.03 mmol) and 1bppCOOEt (8.52 mg, 0.03 mmol) in acetone (1.5 mL) obtaining orange solutions which were stirred for 15 minutes and filtered. In the case of the 1bppCOOH/3bpp-bph combination, the solution was put in contact with diethyl ether vapors yielding a mixture of orange blocks crystals of **1·2Me_2CO·0.5Et_2O** and orange prisms crystals of **1·Me_2CO** after a few days. Besides, pure diethyl ether was layered in a test tube on the 1bppCOOH/1bppCOOEt solution yielding orange prisms of **2·0.5Me_2CO** suitable for X-ray diffraction after one week. Anal. calcd. for $Fe(C_{12}H_9O_4N_5)(C_{35}N_5H_{25})(ClO_4)_2$ (**1**): C 53.38, N 13.24, H 3.24. Found C 53.36, N 13.84, H 3.36 (desolvated sample after heating to 400 K in the SQUID used for magnetic measurements). Anal. Calcd for $Fe(N_5C_{12}H_9O_2)(N_5C_{14}H_{13}O_2)(ClO_4)_2(H_2O)_{0.5}(CH_3COCH_3)_{0.5}$ (**2·0.5Me_2CO**): C, 39.73; H, 3.15; N, 16.85 %. Found: C, 39.96; H, 3.37; N, 16.17 % (compound **2·0.5Me_2CO** absorbs half water molecule in contact with air).

Structural characterization. Single crystals of **1·Me$_2$CO**, **1·2Me$_2$CO·0.5Et$_2$O** or **2·0.5Me$_2$CO** were mounted on a glass fiber using a viscous hydrocarbon oil to coat the crystal and then transferred directly to the cold nitrogen stream for data collection. X-ray data were collected at 120 K for **1·2Me$_2$CO·0.5Et$_2$O**, at 120 and 300 K for **1·Me$_2$CO** and at 120 and 400 K for **2·0.5Me$_2$CO** on a Supernova diffractometer equipped with a graphite-monochromated Enhance (Mo) X-ray Source (λ = 0.71073 Å). Higher temperatures led to the quick loss of crystallinity in **1·Me$_2$CO**. The program CrysAlisPro, Oxford Diffraction Ltd., was used for unit cell determinations and data reduction. Empirical absorption correction was performed using spherical harmonics, implemented in the SCALE3 ABSPACK scaling algorithm. The structures were solved with the ShelXT structure solution program[24] and refined with the SHELXL-2013 program,[25] using Olex2.[26] Non-hydrogen atoms were refined anisotropically, and hydrogen atoms were placed in calculated positions refined using idealized geometries (riding model) and assigned fixed isotropic displacement parameters. Crystallographic data are summarized in Table 1. CCDC-1917750-1917754 contain the supplementary crystallographic data for this paper. These data can be obtained free of charge from The Cambridge Crystallographic Data Centre via www.ccdc.cam.ac.uk/data_request/cif. For powder X-Ray diffraction patterns, a 0.5 mm glass capillary was filled with polycrystalline samples of the complexes and mounted and aligned on an Empyrean PANalytical powder diffractometer, using CuKα radiation (λ = 1.54177 Å). A total of 2 scans were collected for each compound at room temperature in the 2θ range 5-40º.

Table 1. Crystallographic data for compounds **1** and **2**.

Compound	**1·2Me$_2$CO·0.5Et$_2$O**	**1·Me$_2$CO**	**1·Me$_2$CO**	**2·0.5Me$_2$CO**	**2·0.5Me$_2$CO**

Empirical formula	$C_{110}H_{102}Cl_4Fe_2N_{20}O_{25}$	$C_{50}H_{40}Cl_2FeN_{10}O_{11}$	$C_{50}H_{40}Cl_2FeN_{10}O_{11}$	$C_{55}H_{50}Cl_4Fe_2N_{20}O_{25}$	$C_{55}H_{50}Cl_4Fe_2N_{20}O_{25}$
Formula weight	2357.61	1083.67	1083.67	1642.63	1642.63
Crystal colour	Orange	Orange	Orange	Orange	Orange
Crystal size	0.28x0.21x0.16	0.67×0.08× 0.04	0.55×0.25 × 0.12	0.54×0.07× 0.02	0.7 × 0.15 × 0.07
Temperature (K)	120(2)	120(2)	300.00(10)	120(2)	399.95(10)
Wavelength (Å)	0.71073	0.71073	0.71073	0.71073	0.71073
Crystal system	Triclinic	Triclinic	Triclinic	Orthorhombic	Orthorhombic
Space group	*P*-1	*P*-1	*P*-1	*P*bca	*P*bca
a (Å)	10.9594(3)	11.0642(5)	11.2137(6)	14.2991(17)	14.7845(7)
b (Å)	15.2064(5)	13.7718(5)	13.7063(6)	22.0531(11)	22.2028(11)
c (Å)	18.1301(8)	16.4718(9)	16.6716(10)	22.6493(11)	22.5899(13)
α (°)	104.480(3)	79.021(4)	79.292(4)	90	90
ß (°)	94.555(3)	78.129(4)	79.181(5)	90	90
γ (°)	103.052(3)	88.214(3)	86.777(4)	90	90
V (Å^3)	2820.15(18)	2411.2(2)	2472.4(2)	7142.2(10)	7415.3(7)
Z	1	2	2	4	8
ρ_{calc} (Mg/m^3)	1.388	1.493	1.456	1.529	1.457
μ(Mo$_{K\alpha}$) (mm^{-1})	0.433	0.498	0.485	0.647	0.605
2θ range (°)	6.758 to 55.038	6.892 to 55.044	6.786 to 55.988	6.54-55.016	6.622-56.608
Reflns collected	38786	32327	35597	25324	26175
Independent reflns (R_{int})	11731 (0.0609)	10080 (0.0680)	10402 (0.0370)	8178 (0.1448)	7762 (0.1158)
L. S. parameters, *p*/ restraints, *r*	730/0	669/2	661/0	508/0	515/117
$R1(F)$,[a] $I > 2\sigma(I)$	0.0672	0.0552	0.0671	0.1194	0.1114
$wR2(F^2)$,[b] all data	0.1956	0.1410	0.2127	0.3504	0.4133

$S(F^2)$,[c] all data	1.118	1.030	1.048	1.027	0.953

[a]$R1(F) = \sum||F_o|-|F_c||/\sum|F_o|$; [b]$wR2(F^2) = [\sum w(F_o^2-F_c^2)^2/\sum wF_o^4]^{1/2}$; [c]$S(F^2) = [\sum w(F_o^2-F_c^2)^2/\sum n + r - p)]^{1/2}$

Physical characterization. The Fe/Cl ratios were measured with a Philips ESEM X230 scanning electron microscope equipped with an EDAX DX-4 microsonde. Elemental analyses (C, H, and N) were performed with a CE Instruments EA 1110 CHNS Elemental analyzer. Magnetic measurements were performed with a Quantum Design MPMS-XL-5 SQUID magnetometer in the 2 to 400 K temperature range with an applied magnetic field of 0.1 T. Photomagnetic measurements were performed irradiating with a Diode Pumped Solid State Laser DPSS-532-20 from Chylas and a coupled via an optical fiber to the cavity of the SQUID magnetometer. The optical power at the sample surface was adjusted to ~3 $mW \cdot cm^{-2}$, and it was verified that it resulted in no significant change in magnetic response due to heating of the sample. The photomagnetic samples consisted of a thin layer of compound whose weight was corrected by comparison of a thermal spin crossover curve with that of a more accurately weighted sample of the same compound.

Deposition. **1** and **2** were deposited by immersing native SiO_2/Si substrates in 1 mM MeCN solutions of the complexes overnight. Then, they were thoroughly rinsed with MeCN to remove any physisorbed material and then, dried under a N_2 stream. Si substrates covered with a layer of native SiO_2 were obtained from commercial sources (NOVA electronic materials). Atomic Force Microscopy (AFM) was performed with a Digital Instruments Veeco Nanoscope IVa AFM microscope in tapping mode, using silicon tips with natural resonance frequency of 300 kHz and with an equivalent constant force of 40 N/m. Matrix-Assisted Laser Desorption/Ionization Time-Of-Flight (MALDI-TOF) samples were taped to the steel MALDI plate with double side tape. 0.70 µL of Calibration Mixture and CHCA matrix (10 mg/mL HCA (Bruker) in 0.1%

Trifluoroacetic acid-MeCN/H_2O (7:3, v/v)) were spotted onto every slide. The matrix solution was spotted close to the left down part, and the calibration mixture in the opposite side of the slide (0.5 µL of ACH). Slides were allowed to air-dry at room temperature. For every sample a close external calibration was done with CalMix solution spotted at every sample slide. The external calibrated with the calibration mixture spectrum was done by Data Explorer software. The samples mixtures were analyzed in a 5800 MALDI TOFTOF (ABSciex) in positive reflectron mode (3000 shots every position; LASER INTENSITY 5000) in a mass range of 700-4000 m/z; and 200-2000 m/z. X-ray Photoelectron Spectroscopy (XPS) was performed with a K-ALPHA, Thermo Scientific. Samples were analyzed ex situ at the X-ray Spectroscopy Service at the Universidad de Alicante. All spectra were collected using Al Kα radiation (1486.6 eV), monochromatized by a twin crystal monochromator, yielding a focused X-ray spot (elliptical in shape with a major axis length of 400 µm) at 3 mA·C and 12 kV. The alpha hemispherical analyzer was operated in the constant energy mode with survey scan pass energies of 200 eV to measure the whole energy band and 50 eV in a narrow scan to selectively measure the particular elements. XPS data were analyzed with Avantage software. A smart background function was used to approximate the experimental backgrounds. Charge compensation was achieved with the system flood gun that provides low energy electrons and low energy argon ions from a single source. Spectra are referenced using the C 1s main peak (284.8 eV). Soft x-ray absorption (XAS) and x-ray magnetic circular dichroism (XMCD) experiments at the Fe-$L_{2,3}$ edges were performed in the HECTOR cryomagnet endstation at the BL29-BOREAS beamline of the ALBA synchrotron (Barcelona, Spain).[27] The spectra were recorded in TEY method from 4 to 350 K with an energy resolution of ~70 meV, the chamber pressure being lower than $1*10^{-10}$ mbar and photon flux about $5*10^{11}$ s^{-1}. The XMCD spectra were recorded using alternatively left and right circularly polarized x rays produced by an APPLE II undulator and a superconducting split coil setup generating a magnetic field up to 6 T in the direction of propagation of the incident photons.

Results and discussion

Synthesis. The vapor-to-liquid or liquid-to-liquid diffusion of diethyl ether into the solutions resulting from the reaction of $Fe(ClO_4)_2{\cdot}xH_2O$ and equimolar mixtures of 1bppCOOH/3bpp-bph or 1bppCOOH/1bppCOOEt in acetone led to the corresponding heteroleptic compounds $[Fe(1bppCOOH)(3bpp\text{-}bph)](ClO_4)_2{\cdot}2Me_2CO{\cdot}0.5Et_2O$ (**$1{\cdot}2Me_2CO{\cdot}0.5Et_2O$**) and $[Fe(1bppCOOH)(3bpp\text{-}bph)](ClO_4)_2{\cdot}Me_2CO$ (**$1{\cdot}Me_2CO$**) or $[Fe(1bppCOOH)(1bppCOOEt)](ClO_4)_2{\cdot}0.5Me_2CO$ (**$2{\cdot}0.5Me_2CO$**), respectively. In the case of the 1bppCOOH/3bpp-bph combination, the crystal structures of compounds **$1{\cdot}2Me_2CO{\cdot}0.5Et_2O$** and **$1{\cdot}Me_2CO$**, which systematically co-crystallize within the crystallization vial (see experimental section), were successfully determined by single-crystal X-ray diffraction at 120 K (see below). It is important to note that the powder X-ray diffraction (PXRD) pattern of a sample formed by a mixture of the two solvatomorphs at room temperature is consistent with the simulated pattern of **$1{\cdot}Me_2CO$** (see Figure S1). This observation clearly indicates that a partial desolvation of crystals of **$1{\cdot}2Me_2CO{\cdot}0.5Et_2O$** leads to compound **$1{\cdot}Me_2CO$** in contact with air. Indeed, the crystal structure of **$1{\cdot}Me_2CO$** obtained at 300 K confirms that its acetone molecule is not lost at room temperature. At 400 K, compound **$1{\cdot}Me_2CO$** undergoes, after several minutes, a complete loss of crystallinity due to the desorption of the acetone molecules as confirmed by elemental analysis (see experimental section). Consequently, it was not possible to determine the structure of the SCO-active desolvated phase **1** (see below). Powder X-ray diffraction of the SCO phase **1** shows some changes in the position of the peaks with respect to the solvated form (see Figure S1) which suggests sensible structural modifications accompanying to the acetone desorption.

Regarding the heteroleptic complex **2·0.5Me$_2$CO**, the elemental analysis indicates the persistence of the acetone of crystallization found in the structure and also that one water molecule is likely absorbed in contact to air (see experimental section). Besides, the powder X-ray diffraction pattern of **2·0.5Me$_2$CO** is in good agreement with the diagram simulated from the single crystal X-ray diffraction data (see Figure S2).

Structure of [Fe(1bppCOOH)(3bpp-bph)](ClO$_4$)$_2$·2Me$_2$CO·0.5Et$_2$O (1·2Me$_2$CO·0.5Et$_2$O) and [Fe(1bppCOOH)(3bpp-bph)](ClO$_4$)$_2$·Me$_2$CO (1·Me$_2$CO). Both structures, which belong to the triclinic *P*-1 space group, present in the asymmetric unit, one crystallographically independent [Fe(1bppCOOH)(3bpp-bph)]$^{2+}$ complex, two ClO$_4^-$ anions and the corresponding solvent molecules (of acetone and diethyl ether), which in some cases are disordered. The [Fe(1bppCOOH)(3bpp-bph)]$^{2+}$ complex features an iron(II) center coordinated to both mutually perpendicular tridentate ligands (Figure 1) with typical HS Fe-N bond lengths (2.130(3)-2.211(4) Å for **1·2Me$_2$CO·0.5Et$_2$O** at 120 K; 2.131(3)-2.201(3) Å and 2.129(3)-2.197(3) Å for **1·Me$_2$CO** at 120 and 300 K, respectively). The two N-H groups of 3bpp-bph in **1·Me$_2$CO** form hydrogen bonds with the two ClO$_4^-$ anions, while the –OH group from 1bppCOOH is involved in a hydrogen-bond with a disordered acetone molecule (see Figure 1), which has been modeled with two possible configurations with 0.5 occupancies of the two methyl groups and O atom twisted around the central carbonyl C atom. Pairs of [Fe(1bppCOOH)(3bpp-bph)]$^{2+}$ complexes form dimers linked through two symmetrical interactions between one N-H moiety of 3bpp-bph from one complex and the CO group of 1bppCOOH from the other (see Figure S3). Neighboring dimers of **1·Me$_2$CO** present CH$\cdots\pi$ interactions between the two terminal phenyl groups or the central pyridyl rings of 3bpp-bph and the pyrazolyl rings of 1bppCOOH. This leads to chains of dimers running along the *b* axis (see Figure S4). ClO_4^- anions and the acetone molecule occupy the holes between $[Fe(1bppCOOH)(3bpp\text{-}bph)]^{2+}$ complexes. One of the two ClO_4^- anions of **1·Me$_2$CO** is disordered at 300 K. This disorder was solved with two configurations of three of the four oxygen atoms with occupancy fractions of 0.5 per set.

The asymmetric unit of **1·2Me$_2$CO·0.5Et$_2$O** at 120 K contains two acetone molecules and one diethyl ether molecule with an occupancy fraction of 0.5. The hydrogen-bond interactions of $[Fe(1bppCOOH)(3bpp\text{-}bph)]^{2+}$ complexes change with respect to those of **1·Me$_2$CO**. Thus, in **1·2Me$_2$CO·0.5Et$_2$O** the two N-H groups of 3bpp-bph are involved in hydrogen-bonds with an acetone molecule and a ClO_4^- anion, respectively. On the other hand, the OH group of the ligands 1bppCOOH forms a hydrogen-bond with the O atom of the diethyl ether molecule (see Figure S5). Pairs of $[Fe(1bppCOOH)(3bpp\text{-}bph)]^{2+}$ complexes form dimers as those of **1·Me$_2$CO** (see Figure S6), while exhibiting a less compact packing due to the larger number of solvent molecules. This results in an increase of the unit cell volume.

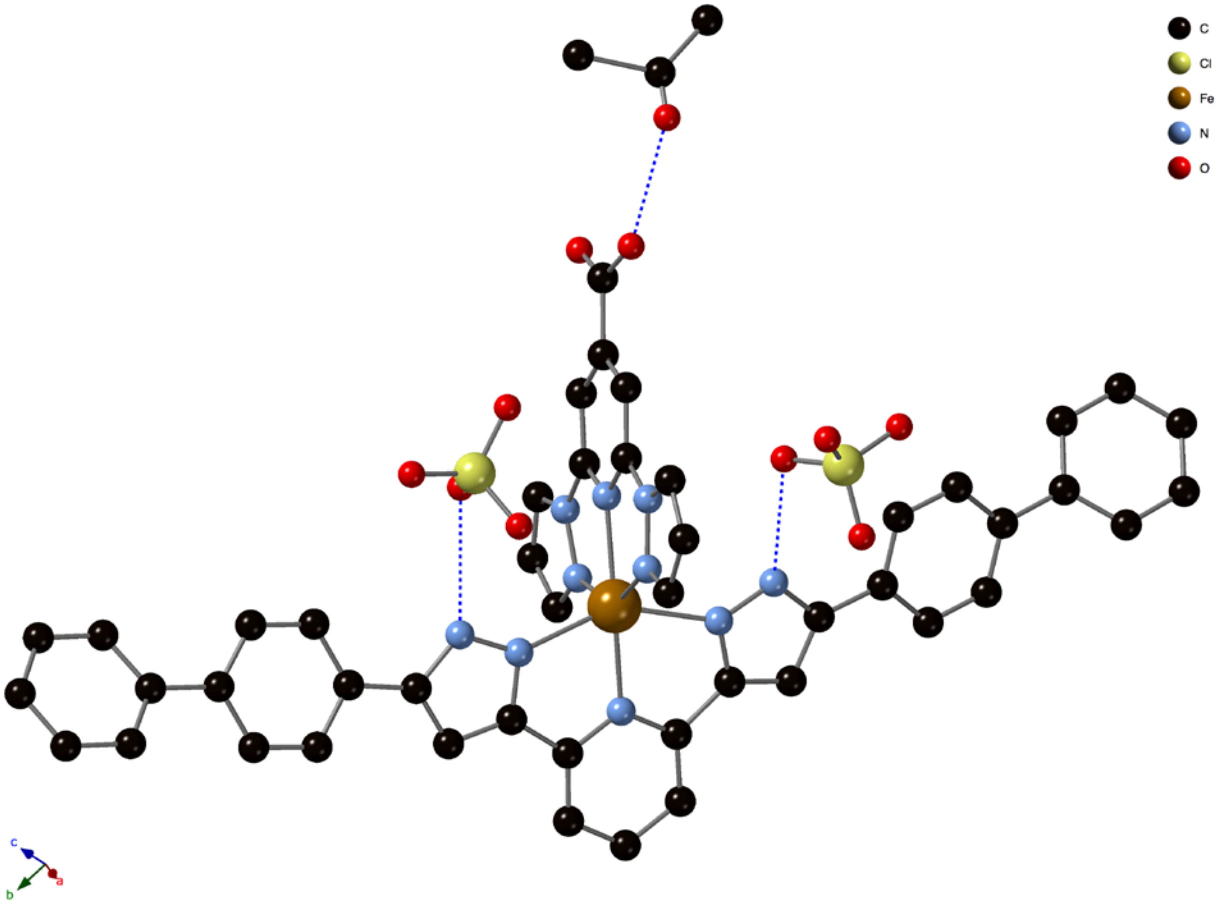

Figure 1. Representation of the molecular units of **1·Me₂CO** at 120 K, Fe (orange) C (black), N (blue), O (red), Cl (yellow). Hydrogen bonds shown with blue dashed lines. Half of the disordered acetone molecules have been omitted for clarity.

Structure of [Fe(bppCOOH)(bppCOOEt)]$(ClO_4)_2$·0.5Me_2CO (2·0.5Me_2CO)

This compound crystallizes in the orthorhombic *P*bca space group. Its structure was solved at 120 and 400 K. The asymmetric unit is composed by one [Fe(1bppCOOH)(1bppCOOEt)]$^{2+}$ cation, three ClO_4^- anions (two of them disordered and with occupancy fractions of 0.5) and one acetone molecule with half occupancy. The central iron(II) ion of the complex is coordinated by six nitrogen atoms from the two tridentate 1bppCOOH and 1bppCOOEt ligands, furnishing a distorted octahedral geometry (Σ = 85.200(5)° and θ = 281.222(8)° at 120 K and Σ = 109° and θ = 358° at 400 K where $\Sigma = \sum_{i=1}^{12} \left|90 - \alpha i\right|$ where α_i are the12 cis-N-Fe-N angles around the iron atom and $\Theta = \sum_{j=1}^{24} \left|60 - \theta j\right|$ where θj are the 24 unique N-Fe-N around the iron atom), confirming the formation of the heteroleptic complex (see Figure 2). Fe–N bond lengths at 120 K range from 1.892(8) to 1.976(8) Å, which are typical LS Fe–N lengths for an octahedral Fe(II) complex. At 400 K, an increase in the Fe–N bond lengths [which lie in the range 1.948(7) to 2.037(10) Å)] is observed. These distances are intermediate between the expected LS and HS ones, confirming the partial spin crossover observed in the magnetic measurements (see below). Also, the disorder increases at this temperature (on the ClO_4^- anions, the carboxylic acid substituents and ethyl carboxylate groups of 1bppCOOH and 1bppCOOEt, respectively) as expected, but the fractional acetone molecule is still present.

The acetone molecules form hydrogen bonds with the ligand 1bppCOOH (d_{O2_O15} = 2.68 Å at 120 K, see Figure 2) preventing the formation of hydrogen bonds between neighboring complexes as observed in the homoleptic $[Fe(1bppCOOH)_2](ClO_4)_2$ and $[Fe(1bppCOOH)_2](BF_4)_2$ salts.[19,21] Neighboring $[Fe(1bppCOOH)(1bppCOOEt)]^{2+}$ complexes present CH$\cdots\pi$ contacts between CH groups and aromatic rings from the pyrazolyl groups of ligand 1bppCOOH. This gives rise to chains of complexes running along the *a* axis (see Figure S7). These chains, which are surrounded by ClO_4^- anions and acetone molecules, are connected through short contacts involving CO groups from 1bppCOOH and 1bppCOOEt and CH groups from pyridine and pyrazolyl groups from both ligands (see Figure S7).

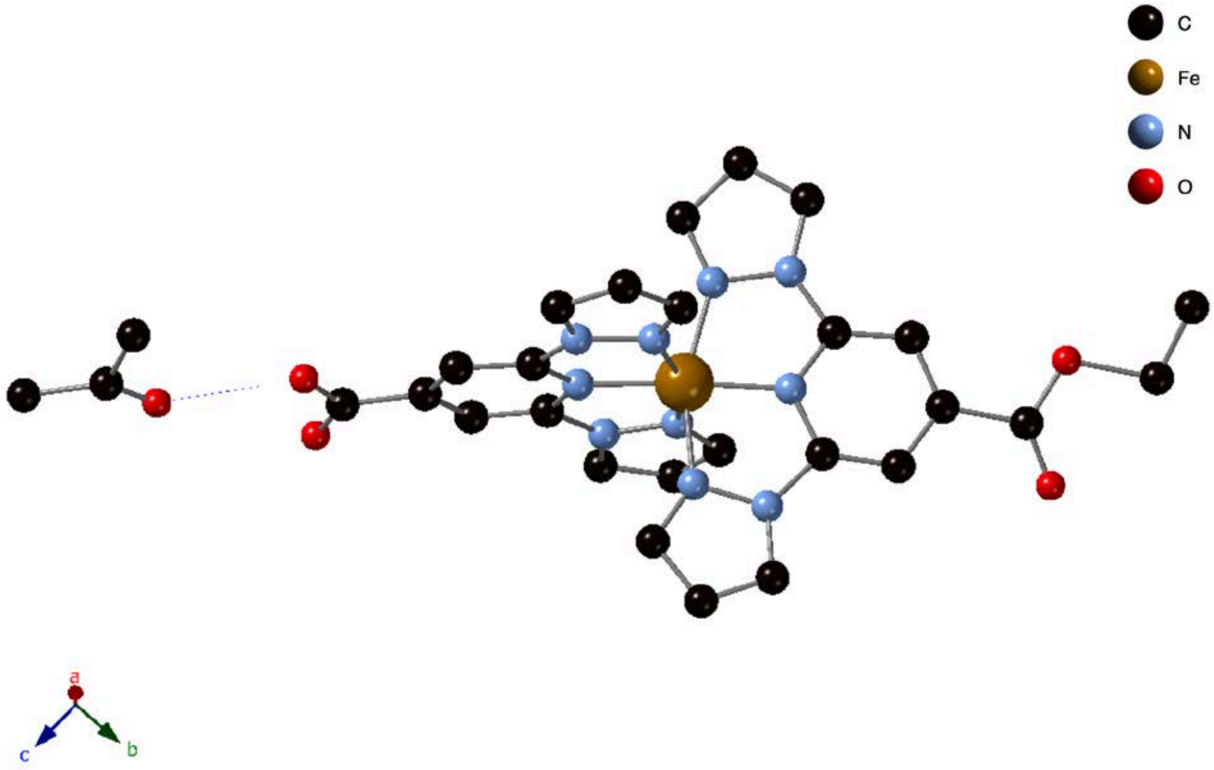

Figure 2. Representation of $[Fe(bppCOOH)(bppCOOEt)]^{2+}$ and acetone molecule in **2·0.5Me$_2$CO** at 120 K, Fe (orange) C (black), N (blue), O (red). Hydrogen bond shown with blue dashed lines. Half of the disordered acetone molecules have been omitted for clarity.

Magnetic properties. The temperature dependence of the product $\chi_M T$ (χ_M is the molar paramagnetic susceptibility) of the mixture of filtered crystals of **1·2Me$_2$CO·0.5Et$_2$O** and **1·Me$_2$CO** is shown in Figure 3. As mentioned above, the PXRD pattern at room temperature indicates that the structure of this sample is that of **1·Me$_2$CO**. The value of χ_MT is close to 3.4-3.6 cm^3·K·mol^{-1} in the 50 to 400 K range, consistent with the HS state of **1·Me$_2$CO** at 120 and 300 K, as indicated by the Fe-N distances from the molecular structure (see above). The sharp decrease below 50 K is due to zero-field-splitting as expected for the Fe(II) ion in the HS state. Quite remarkably, after heating to 400 K, the desolvated phase (**1**) shows a completely different behavior. Thus, when cooling from 300 to 250 K, a gradual decrease of $\chi_M T$ from 3.3 $cm^3 \cdot K \cdot mol^{-1}$ at 300 K to 2.75 $cm^3 \cdot K \cdot mol^{-1}$ at 250 K is registered. Upon further cooling, an abrupt decrease of the $\chi_M T$ value is observed down to 0.9 $cm^3 \cdot K \cdot mol^{-1}$ at 220 K. Below this temperature, the χ_MT product decreases gradually registering a value of 0.5 $cm^3 \cdot K \cdot mol^{-1}$ at 50 K that indicates an almost complete spin transition. The lowest temperature $\chi_M T$ value is consistent with a ~15% of residual Fe(II) ions in the HS state. The latter behavior is observed persistently upon repeated cycles in the heating and cooling modes with a small thermal hysteresis of 13 K ($T_{1/2}\downarrow$ = 234 K and $T_{1/2}\uparrow$ = 247 K, $T_{1/2}$ = temperature of 50 % HS to LS conversion). The presence of this thermal hysteresis loop clearly demonstrates the existence of a significant level of cooperativity in the desolvated sample. Although it is difficult to rationalize this behavior without knowing the structure of the desolvated phase, several explanations are possible. On the one hand, the removal of the acetone solvent molecule could change the hydrogen-bonding to the NH groups of 3bpp-bph as observed with the partial desolvation from **$1 \cdot 2Me_2CO \cdot 0.5Et_2O$** to **$1 \cdot Me_2CO$.** This would change the crystal field around iron(II), taking into account that the spin state of 3bpp iron(II) complexes is very sensitive to hydrogen-bonded solvent molecules or counteranions.[9,12–14,28] On the other hand, the larger chemical pressure induced by the decrease in unit cell volume after removal of the solvent molecules could stabilize the LS state.

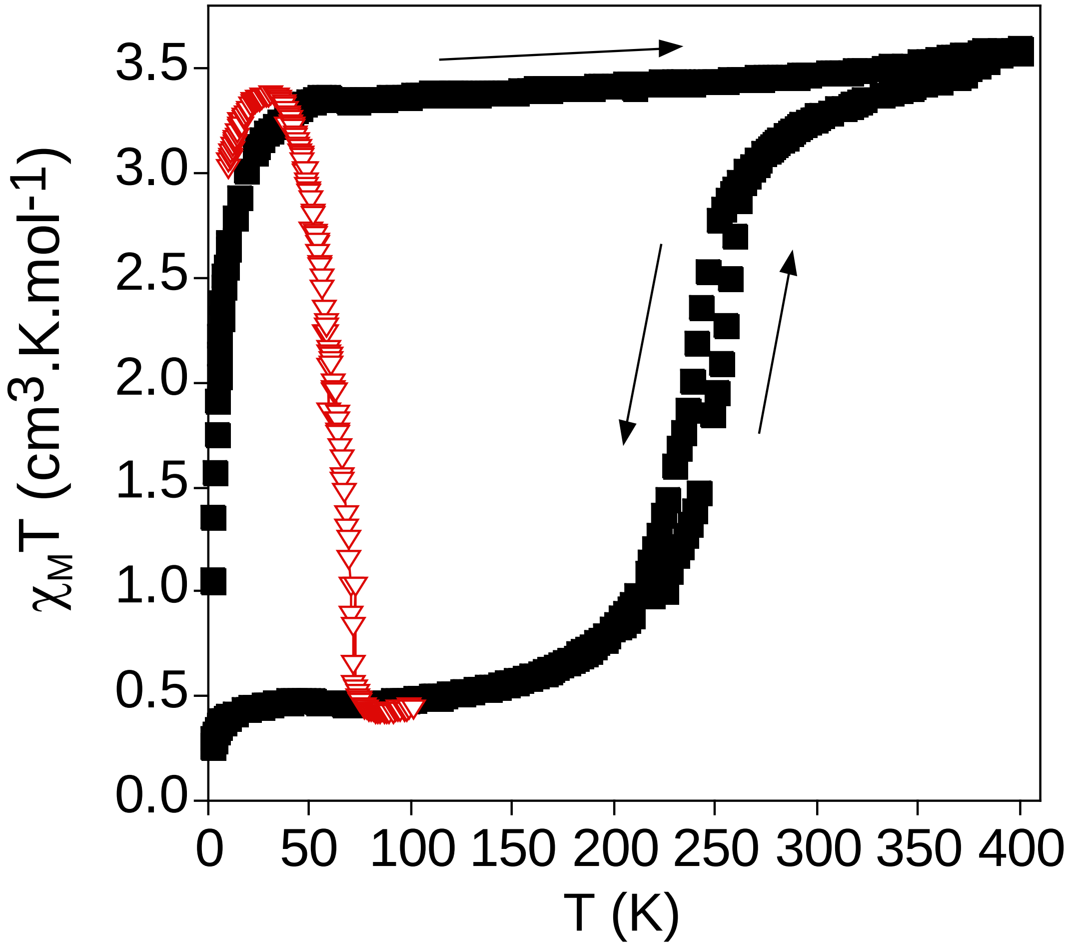

Figure 3. Thermal variation of χ_MT for **1·Me₂CO**. Full black squares: data recorded without irradiation; empty red triangles: data recorded after irradiation at 10 K.

The temperature dependence of the $\chi_M T$ value for **2·0.5Me₂CO** is shown in Figure 4. From 2 to 300 K, $\chi_M T$ values are lower than 0.4 cm^3·K·mol^{-1}, consistent with an iron(II) ion being in the LS state, in agreement with the Fe-N distances found at 120 K (see above). At higher temperatures, a gradual increase of the magnetic signal to reach a χ_MT value of 1.6 cm^3·K·mol^{-1}

at 400 K is recorded. Therefore, an spin transition takes place in this compound with a *T*$_{1/2}$ well above 300 K and close to 400 K that is not completed at the latter temperature (the highest measured). This behavior is reversible in the cooling cycle after heating to 400 K (Figure S8). This is consistent with the structural data that indicates that heating at 400 K does not remove the half equivalent of acetone molecules found in the structure.

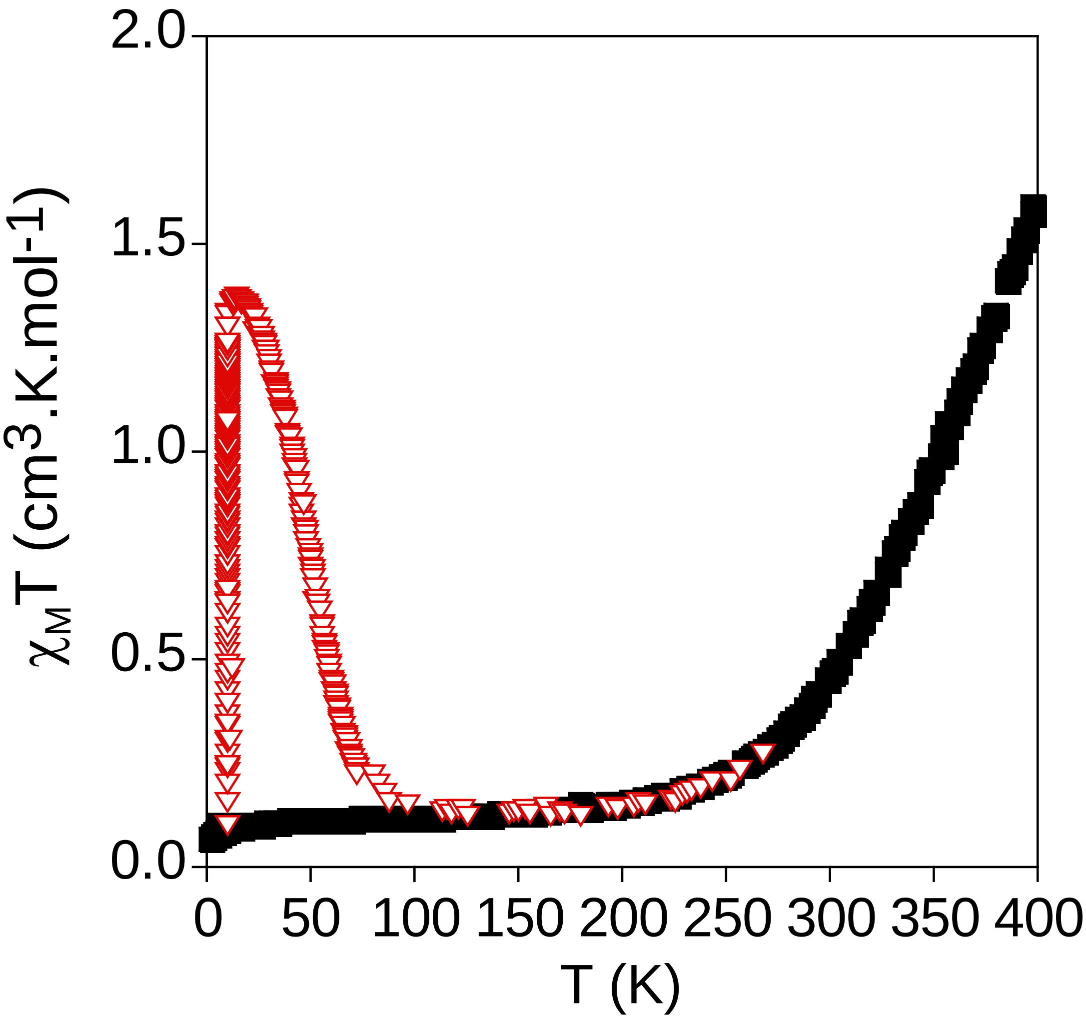

Figure 4. Thermal variation of $\chi_M T$ for **$2 \cdot 0.5Me_2CO$**. Full Black squares: data recorded without irradiation; empty red triangles: data recorded after irradiation at 10 K.

Photomagnetic properties. Compound **1**, after previous desolvation at 400 K in the SQUID device, was irradiated with a 532 nm laser at 10 K, causing a drastic increase of the magnetic signal. Once the irradiation was switched off, the temperature was increased at 0.3 $K \cdot min^{-1}$ while the magnetic susceptibility was recorded (see Figure 3). In the 10−31 K temperature range, an increase of $\chi_M T$ to reach a maximum value of 3.4 $cm^3 \cdot K \cdot mol^{-1}$ at 31 K was observed, reflecting a zero-field splitting of HS Fe(II) and suggesting an almost quantitative LS to HS photoconversion. The *T*(LIESST), defined as the minimum of the derivative of $\chi_M T$ with temperature, is 71 K. Compound **2** also displays a clear increase of the magnetic susceptibility after light irradiation (532 nm). In contrast to **1**, a complete photoconversion of **2** is not achieved. Thus, a maximum $\chi_M T$ value of 1.4 $cm^3 \cdot K \cdot mol^{-1}$ at 15 K is observed, consistent with a ~40 % photoconversion with a *T*(LIESST) of 52 K. On the other hand, while **1** shows an abrupt LIESST relaxation curve, **2** exhibits a more gradual LIESST curve, which could be attributed to the weaker intermolecular interactions of this last compound and/or to the incomplete photoswitching. The *T*(LIESST) of **1** and **2** mirror the linear correlation between the thermal spin crossover temperature ($T_{1/2}$) and the *T*(LIESST) found for this family of compounds and described by the formula $T(\text{LIESST}) = T_0 - 0.3T_{1/2}$ (T_0 = 150 K).[12–14,29–32] While, *T*(LIESST) and $T_{1/2}$ of **1** fit well with this formula, data of **2** present a small deviation, being *T*(LIESST) around 20 K higher than expected. This deviation may in part be caused by the fact that it was not possible to measure the whole SCO process of **2** within the experimentally accessible temperature range. It is however consistent with the behavior observed in other compounds with $T_{1/2}$ well above room temperature, which also deviate from this formula.[21,33–35]

Deposition on substrates. The grafting of molecules functionalized with carboxylic acid groups onto metal-oxide surfaces is a well-known process.[36–40] **1** and **2** were deposited by immersing the SiO_2/Si substrates in 1 mN acetonitrile solutions of the complexes overnight. The deposited complexes were preliminary characterized by XPS, AFM, Matrix-Assisted Laser Desorption/Ionization Time-Of-Flight (MALDI-TOF) and XAS experiments. SiO_2/Si substrates were used because they are model surfaces for CMOS (Complementary metal–oxide–semiconductor) applications. AFM measurements show a small increase of roughness with respect to the naked substrate after deposition with maximum height differences consistent with the length of the molecule (1.2 nm for $[Fe(1bppCOOH)(3bpp\text{-}bph)]^{2+}$ and 1.6 nm for $[Fe(1bppCOOH)(1bppCOOEt)]^{2+}$ calculated from the single crystal X-ray diffraction structure) (Figure S9). From these results, the level of deposition (monolayer or submonolayer coverage) could not be completely identified but they confirm the absence of deposition of aggregates or multilayers. This is not unexpected considering that the carboxylic acid groups promote the grafting of the first layer of the complexes on the oxide surfaces, whereas additional layers would be removed after rinsing with MeCN, since they are not chemically bonded to the substrate. MALDI-TOF was used to test the presence of the two ligands of the heteroleptic complexes on the surface. Peaks corresponding to protonated 1bppCOOH and 3bpp-bph were obtained in the case of **1** and only 1bppCOOH in **2**. In the case of the 1bppCOOEt, this species could not be clearly identified without ambiguity as a result of interfering peaks coming from the polymer matrix used during the experiments (Figure S10). The presence of Fe(II) on the surface was verified by two other techniques. As is common in the characterization of SAMs, only a combination of techniques proves the quality of the molecular layer. Survey XPS spectra present the characteristic signals of the expected elements (C, N, Si, Fe, O) except that of Cl (Figures S11 and S12). Therefore, the presence of anionic charges in the surface compensates the positive charge of the complexes. Another possible explanation is that the carboxylic acid groups of 1bppCOOH ligand are deprotonated after grafting. High resolution N 1s and Fe 2p XPS spectra are consistent with the presence of pyridine and pyrazole rings of the ligands and iron (Figures S11 and S12 and associated text). XAS experiments were chosen to determine the spin and oxidation state of iron in [Fe(1bppCOOH)(3bpp-bph)]$^{2+}$ and [Fe(1bppCOOH)(1bppCOOEt)]$^{2+}$ deposited on the substrates. This technique gives a straightforward identification of the HS and LS and oxidation state, while the surface sensitivity is warranted by the adopted detection mode, i.e. the Total Electron Yield (TEY) mode. Indeed, it has already been used to characterize the spin state of sub- and monolayers of SCO complexes evaporated on different surfaces.[41–48] At 300 K, the spectrum of deposited [Fe(1bppCOOH)(3bpp-bph)]$^{2+}$ shows a main resonance at the L_3-edge at 710.0 eV with a shoulder at 708.5 eV and two relatively weaker resonant features in the L_2-edge region (719-725 eV) (Figure S13). These energies, line shapes and branching ratios are characteristic of HS Fe(III) complexes.[49–53] XAS spectra of deposited [Fe(1bppCOOH)(1bppCOOEt)]$^{2+}$ at 300 and 4 K present similar features at the L_3 edge but with a higher shoulder-to-peak ratio of intensities at lower energies (Figure S14). These measurements show an irreversible increase of the intensity of the shoulder at 708.5 V under continuous illumination with the x-ray beam (see Figures S13 and S14). This could be related to photoreduction of Fe(III) to Fe(II) as a result of the local electric fields built up in the interface under soft X-ray sources in low conducting substrates.[54] This effect could be reduced by decreasing the photon flux to around 80 % of its initial intensity (**1**) and decreasing the temperature in the case of **2**. These spectra differ drastically from those obtained in the bulk compound [Fe(1bppCOOH)$_2$](BF$_4$)$_2$ measured at 100 and 350 K,[21] which has been used as reference compound for the LS and HS states of Fe(II), respectively (see Figure S15 and associated text). Therefore, XAS results suggests that [Fe(1bppCOOH)(3bpp-bph)]$^{2+}$ and [Fe(1bppCOOH)(1bppCOOEt)]$^{2+}$ decompose on the surface after the metal ions oxidize from Fe(II) to Fe(III) (or under the measurement conditions) taking into account that octahedral bis(tridentate) Fe(III) complexes of 1bpp derivatives are not stable. Preliminary results with homoleptic Fe(II) complexes of 1bppCOOH and 1bpp derivatives on Si/SiO$_2$, Al$_2$O$_3$, ITO or Au gave similar results with a variable degree of photoreduction, which increases in the less conducting substrates. All these results could indicate that this type of ligands bind iron too weakly to be deposited as observed previously for 1bpp complexes containing sulfur substituents on gold.[55] The use of other deposition conditions such as less polar solvents or increased concentrations of the complexes, and the preparation of more robust Fe(II) complexes based on other 1bpp derivatives could be possible strategies to improve these results.

Conclusions

The preparation of two new heteroleptic complexes [Fe(1bppCOOH)(L)](ClO$_4$)$_2$ (L=3bpp-bph (**1**) or 1bppCOOEt (**2**)), in addition to those previously reported, confirms a clear tendency for the formation of the mixed ligand species over the homoleptic ones. This constitutes a rich resource in the search of better performing SCO complexes. The combination in compound **1** of 1bppCOOH and 3bpp-bph ligands has resulted in an improvement of the SCO properties with respect to the homoleptic [Fe(1bppCOOH)$_2$]$^{2+}$ compound since a hysteretic thermal SCO closer to room temperature has been achieved. Besides, compound **2** represents the first heteroleptic complex based on two 1bpp type ligands. In this case, the combination of 4’ substituted 1bpp type ligands stabilizes, as it occurs in the corresponding homoleptic compounds ([Fe(1bppCOOH)$_2$](ClO$_4$)$_2$ and [Fe(1bppCOOEt)$_2$](ClO$_4$)$_2$), the LS state. Moreover, both **1** and **2** complexes exhibit the LIESST effect at 10 K with a 532 nm laser, which further proves that the preparation of heteroleptic complexes is a suitable strategy for obtaining new SCO materials with improved properties.

Finally, an interesting feature of these heteroleptic complexes is the presence of 1bpp ligands functionalized with a carboxylic acid group in the 4-pyridyl position. This paves the way for the preparation of new heteroleptic SCO complexes combining different properties in the two ligands by exploiting the chemical versatility of 1bpp, which can be functionalized in this position with a variety of functional substituents without perturbing significantly the SCO properties.

ASSOCIATED CONTENT

Supporting Information. Structural views of the structures, Powder X ray diffraction patterns of the compounds, magnetic measurements of **2·0.5Me$_2$CO**, AFM, MALDI-TOF, XPS and XAS of the deposited complexes. This material is available free of charge via the Internet at http://pubs.acs.org.

AUTHOR INFORMATION

Corresponding Authors

E-mail for C. B. –M.: Carlos.Bartual@uv.es

E-mail for G. A.: guillem.aromi@qi.ub.edu

E-mail for M. C. -L.: miguel.clemente@uv,es

ACKNOWLEDGMENT

Financial support from the EU (ERC Advanced Grant MOL-2D 788222), the Spanish Ministerio de Economía y Competitividad (MINECO) and FEDER funds (CTQ2015-68370-P, MAT-2017-89993-R, CTQ2016-78341-P and Unidad de Excelencia María de Maeztu MDM-2015-0538) and the Generalitat Valenciana (PROMETEO/2016/147) is gratefully acknowledged. We thank J. M. Martínez-Agudo and G. Agustí from the Universidad de Valencia for the magnetic measurements and. Fernando Coloma from Universidad de Alicante for XPS measurements. The proteomic analysis was performed in the proteomics facility of SCSIE University of Valencia. This proteomics laboratory is a member of Proteored, PRB3 and is supported by grant PT17/0019, of the PE I+D+i 2013-2016, funded by ISCIII and ERDF. XAS and XPS experiments were performed at BL29-BOREAS beamline at ALBA Synchrotron with the collaboration of ALBA staff.

REFERENCES

(1) Gütlich, P.; Goodwin, H. A (eds). *Spin Crossover in Transition Metal Compounds*. *Top Curr. Chem.* **2004**. vol. *233-235*.

(2) Halcrow, M. A (ed). *Spin-Crossover Materials: Properties and Applications*; John Willey & Sons, Chichester, UK, **2013**.

(3) Senthil Kumar, K.; Ruben, M. Emerging Trends in Spin Crossover (SCO) Based Functional Materials and Devices. *Coord. Chem. Rev*. **2017,** *346*, 176–205.

(4) Halcrow, M. A. The Synthesis and Coordination Chemistry of 2,6-

Bis(Pyrazolyl)Pyridines and Related Ligands — Versatile Terpyridine Analogues. *Coord. Chem. Rev.* **2005**, *249* (24), 2880–2908.

(5) Halcrow, M. A. Iron(II) Complexes of 2,6-Di(Pyrazol-1-yl)Pyridines—A Versatile System for Spin-Crossover Research. *Coord. Chem. Rev.* **2009**, *253* (21–22), 2493–2514.

(6) Olguín, J.; Brooker, S. Spin Crossover Active Iron(II) Complexes of Selected Pyrazole-Pyridine/Pyrazine Ligands. *Coord. Chem. Rev.* **2011**, *255* (1–2), 203–240.

(7) Halcrow, M. A. Recent Advances in the Synthesis and Applications of 2,6-Dipyrazolylpyridine Derivatives and Their Complexes. *New J. Chem.* **2014**, *38* (5), 1868–1882.

(8) Kershaw Cook, L. J.; Mohammed, R.; Sherborne, G.; Roberts, T. D.; Alvarez, S.; Halcrow, M. A. Spin State Behavior of Iron(II)/Dipyrazolylpyridine Complexes. New Insights from Crystallographic and Solution Measurements. *Coord. Chem. Rev.* **2015**, *289–290*, 2–12.

(9) Craig, G. A.; Roubeau, O.; Aromí, G. Spin State Switching in 2,6-Bis(Pyrazol-3-yl)Pyridine (3-Bpp) Based Fe(II) Complexes. *Coord. Chem. Rev.* **2014**, *269*, 13–31.

(10) Decurtins, S.; Gütlich, P.; Köhler, C. P.; Spiering, H.; Hauser, A. Light-Induced Excited Spin State Trapping in a Transition-Metal Complex: The Hexa-1-Propyltetrazole-Iron (II) Tetrafluoroborate Spin-Crossover System. *Chem. Phys. Lett.* **1984**, *105* (1), 1–4.

(11) Hauser, A. Light-Induced Spin Crossover and the High-Spin-Low-Spin Relaxation; *Top Curr. Chem.* **2004**, *234*, 155-198.

(12) Marcen, S.; Lecren, L.; Capes, L.; Goodwin, H. A.; Létard, J.-F. Critical Temperature of the LIESST Effect in a Series of Hydrated and Anhydrous Complex Salts Fe(bpp)$_2$X$_2$. *Chem. Phys. Lett*. **2002**, *358*, 87–95

(13) Buchen, T.; Gütlich, P.; Sugiyarto, K. H.; Goodwin, H. A. High-Spin - Low-Spin Relaxation in [Fe(Bpp)$_2$](CF$_3$SO$_3$)$_2$ H$_2$O after LIESST and Thermal Spin-State Trapping—Dynamics of Spin Transition Versus Dynamics of Phase Transition. *Chem. Eur. J.* **1996**, *2* (9), 1134–1138.

(14) Roberts, T. D.; Tuna, F.; Malkin, T. L.; Kilner, C. A.; Halcrow, M. A. An Iron(II) Complex Exhibiting Five Anhydrous Phases, Two of Which Interconvert by Spin-Crossover with Wide Hysteresis. *Chem. Sci.* **2012**, *3* (2), 349–354.

(15) Costa, J. S.; Rodríguez-Jiménez, S.; Craig, G. A.; Barth, B.; Beavers, C. M.; Teat, S. J.; Aromí, G. Three-Way Crystal-to-Crystal Reversible Transformation and Controlled Spin Switching by a Nonporous Molecular Material. *J. Am. Chem. Soc.* **2014**, *136* (10), 3869–3874.

(16) Barrios, L. A.; Bartual-Murgui, C.; Peyrecave-Lleixà, E.; Le Guennic, B.; Teat, S. J.; Roubeau, O.; Aromí, G. Homoleptic versus Heteroleptic Formation of Mononuclear Fe(II) Complexes with Tris-Imine Ligands. *Inorg. Chem.* **2016**, *55* (9), 4110–4116.

(17) Aromí, G.; Beavers, C. M.; Sánchez Costa, J.; Craig, G. A.; Mínguez Espallargas, G.; Orera, A.; Roubeau, O. Snapshots of a Solid-State Transformation: Coexistence of Three Phases Trapped in One Crystal. *Chem. Sci.* **2016**, *7* (4), 2907–2915.

(18) Bartual-Murgui, C.; Diego, R.; Vela, S.; Teat, S. J.; Roubeau, O.; Aromí, G. A Spin-

Crossover Molecular Material Describing Four Distinct Thermal Pathways. *Inorg. Chem.* **2018**, *57*, 11019–11026.

(19) Abhervé, A.; Clemente-León, M.; Coronado, E.; Gómez-García, C. J.; López-Jordà, M. A Spin-Crossover Complex Based on a 2,6-Bis(Pyrazol-1-yl)Pyridine (1-Bpp) Ligand Functionalized with a Carboxylate Group. *Dalton Trans.* **2014**, *43* (25), 9406–9409.

(20) Abhervé, A.; Recio-Carretero, M. J.; López-Jordà, M.; Clemente-Juan, J. M.; Canet-Ferrer, J.; Cantarero, A.; Clemente-León, M.; Coronado, E. Nonanuclear Spin-Crossover Complex Containing Iron(II) and Iron(III) Based on a 2,6-Bis(Pyrazol-1-yl)Pyridine Ligand Functionalized with a Carboxylate Group. *Inorg. Chem.* **2016**, *55* (18), 9361–9367.

(21) García-López, V.; Palacios-Corella, M.; Abhervé, A.; Pellicer-Carreño, I.; Desplanches, C.; Clemente-León, M.; Coronado, E. Spin-Crossover Compounds Based on Iron(Ii) Complexes of 2,6-Bis(Pyrazol-1-yl)Pyridine (bpp) Functionalized with Carboxylic Acid and Ethyl Carboxylic Acid. *Dalton Trans.* **2018**, *47* (47), 16958–16968.

(22) Senthil Kumar, K.; Heinrich, B.; Vela, S.; Moreno-Pineda, E.; Bailly, C.; Ruben, M. Bi-Stable Spin-Crossover Characteristics of a Highly Distorted [Fe(1-BPP-COOC_2H_5)$_2$](ClO $_4$)$_2$·CH_3CN Complex. *Dalton Trans.* **2019**, *48* (12), 3825–3830.

(23) Vermonden, T.; Branowska, D.; Marcelis, A. T. M.; Sudhölter, E. J. R. Synthesis of 4-Functionalized Terdendate Pyridine-Based Ligands. *Tetrahedron* **2003**, *59* (27), 5039–5045.

(24) Sheldrick, G. M.; IUCr. A Short History of *SHELX*. *Acta Crystallogr. Sect. A Found.*

Crystallogr. **2008**, *64* (1), 112–122.

(25) Sheldrick, G. M. Crystal Structure Refinement with *SHELXL*. *Acta Crystallogr. Sect. C Struct. Chem.* **2015**, *71* (1), 3–8.

(26) Bourhis, L. J.; Dolomanov, O. V.; Gildea, R. J.; Howard, J. A. K.; Puschmann, H. The Anatomy of a Comprehensive Constrained, Restrained Refinement Program for the Modern Computing Environment – *Olex2* Dissected. *Acta Crystallogr. Sect. A Found. Adv.* **2015**, *71* (1), 59–75.

(27) Barla, A.; Nicolás, J.; Cocco, D.; Valvidares, S. M.; Herrero-Martín, J.; Gargiani, P.; Moldes, J.; Ruget, C.; Pellegrin, E.; Ferrer, S. Design and Performance of BOREAS, the Beamline for Resonant X-Ray Absorption and Scattering Experiments at the ALBA Synchrotron Light Source. *J. Synchrotron Radiat.* **2016**, *23* (6), 1507–1517.

(28) Giménez-López, M. del C.; Clemente-León, M.; Giménez-Saiz, C. Unravelling the Spin-State of Solvated $[Fe(Bpp)_2]^{2+}$ Spin-Crossover Complexes: Structure–function Relationship. *Dalton Trans.* **2018**, *47* (31), 10453–10462.

(29) Létard J-F.; Guionneau P.; Rabardel, L.; Howard, J. A. K.; Goeta, A. E.; Chasseau, D. Kahn O. Structural, Magnetic, and Photomagnetic Studies of a Mononuclear Iron(II) Derivative Exhibiting an Exceptionally Abrupt Spin Transition. Light-Induced Thermal Hysteresis Phenomenon. *Inorg. Chem.* **1998**, *37* (17), 4432-4441.

(30) Létard, J.-F.; Capes, L.; Chastanet, G.; Moliner, N.; Létard, S.; Real, J.-A.; Kahn, O. Critical Temperature of the LIESST Effect in Iron(II) Spin Crossover Compounds. *Chem. Phys. Lett.* **1999**, *313* (1–2), 115–120.

(31) Létard, J.-F.; Guionneau, P.; Nguyen, O.; Costa, J. S.; Marcén, S.; Chastanet, G.; Marchivie, M.; Goux-Capes, L. A Guideline to the Design of Molecular-Based Materials with Long-Lived Photomagnetic Lifetimes. *Chem. Eur. J.* **2005**, *11* (16), 4582–4589.

(32) Létard, J.-F. Photomagnetism of Iron(II) Spin Crossover Complexes—the T(LIESST) Approach. *J. Mater. Chem.* **2006**, *16* (26), 2550–2559.

(33) Pritchard, R.; Lazar, H.; Barrett, S. A.; Kilner, C. A.; Asthana, S.; Carbonera, C.; Létard, J.-F.; Halcrow, M. A. Thermal and Light-Induced Spin-Transitions in Iron(II) Complexes of 2,6-Bis(4-Halopyrazolyl)Pyridines: The Influence of Polymorphism on a Spin-Crossover Compound. *Dalton Trans.* **2009**, No. 33, 6656.

(34) Sánchez-Sánchez, C.; Desplanches, C.; Clemente-Juan, J. M.; Clemente-León, M.; Coronado, E. Photomagnetic Properties of an Fe(II) Spin-Crossover Complex of 6-(3,5-Diamino-2,4,6-Triazinyl)-2,2'-Bipyridine and Its Insertion into 2D and 3D Bimetallic Oxalate-Based Networks. *Dalton Trans.* **2017**, *46* (8), 2680–2689.

(35) Rigamonti, L.; Bridonneau, N.; Poneti, G.; Tesi, L.; Sorace, L.; Pinkowicz, D.; Jover, J.; Ruiz, E.; Sessoli, R.; Cornia, A. A Pseudo-Octahedral Cobalt(II) Complex with Bispyrazolylpyridine Ligands Acting as a Zero-Field Single-Molecule Magnet with Easy Axis Anisotropy. *Chem. Eur. J.* **2018**, *24* (35), 8857–8868.

(36) Wei, T.-X.; Shi, Y.-R.; Zhai, J.; Gan, L.-B.; Huang, C.-H.; Liu, T.-T.; Ying, L.-M.; Luo, G.-B.; Zhao, X.-S. Synthesis, Monolayer Fabrication and Photoelectric Conversion Property of Two Pyrrolidinofullerene Carboxylic Acid Derivatives. *Chem. Phys. Lett.* **2000**, *319* (1–2), 7–12.

(37) Mottaghi, M.; Horowitz, G. Field-Induced Mobility Degradation in Pentacene Thin-Film Transistors. *Org. Electron.* **2006**, *7* (6), 528–536.

(38) Mottaghi, M.; Lang, P.; Rodriguez, F.; Rumyantseva, A.; Yassar, A.; Horowitz, G.; Lenfant, S.; Tondelier, D.; Vuillaume, D. Low-Operating-Voltage Organic Transistors Made of Bifunctional Self-Assembled Monolayers. *Adv. Funct. Mater.* **2007**, *17* (4), 597–604.

(39) Bertazzo, S.; Rezwan, K. Control of α-Alumina Surface Charge with Carboxylic Acids. *Langmuir* **2010**, *26* (5), 3364–3371.

(40) Choi, J.-H.; Kim, S.-O.; Linardy, E.; Dreaden, E. C.; Zhdanov, V. P.; Hammond, P. T.; Cho, N.-J. Adsorption of Hyaluronic Acid on Solid Supports: Role of PH and Surface Chemistry in Thin Film Self-Assembly. *J. Colloid Interface Sci.* **2015**, *448*, 197–207.

(41) Miyamachi, T.; Gruber, M.; Davesne, V.; Bowen, M.; Boukari, S.; Joly, L.; Scheurer, F.; Rogez, G.; Yamada, T. K.; Ohresser, P.; et al. Robust Spin Crossover and Memristance across a Single Molecule. *Nat. Commun.* **2012**, *3* (1), 938.

(42) Bernien, M.; Wiedemann, D.; Hermanns, C. F.; Krüger, A.; Rolf, D.; Kroener, W.; Müller, P.; Grohmann, A.; Kuch, W. Spin Crossover in a Vacuum-Deposited Submonolayer of a Molecular Iron(II) Complex. *J. Phys. Chem. Lett.* **2012**, *3* (23), 3431–3434.

(43) Gopakumar, T. G.; Bernien, M.; Naggert, H.; Matino, F.; Hermanns, C. F.; Bannwarth, A.; Mühlenberend, S.; Krüger, A.; Krüger, D.; Nickel, F.; et al. Spin-Crossover Complex on Au(111): Structural and Electronic Differences Between Mono- and Multilayers.

Chem. Eur. J. **2013**, *19* (46), 15702–15709.

(44) Warner, B.; Oberg, J. C.; Gill, T. G.; El Hallak, F.; Hirjibehedin, C. F.; Serri, M.; Heutz, S.; Arrio, M.-A.; Sainctavit, P.; Mannini, M.; et al. Temperature- and Light-Induced Spin Crossover Observed by X-Ray Spectroscopy on Isolated Fe(II) Complexes on Gold. *J. Phys. Chem. Lett.* **2013**, *4* (9), 1546–1552.

(45) Beniwal, S.; Zhang, X.; Mu, S.; Naim, A.; Rosa, P.; Chastanet, G.; Létard, J.-F.; Liu, J.; Sterbinsky, G. E.; Arena, D. A.; et al. Surface-Induced Spin State Locking of the $[Fe(H_2B(Pz)_2)_2(Bipy)]$ Spin Crossover Complex. *J. Phys. Condens. Matter* **2016**, *28* (20), 206002.

(46) Ossinger, S.; Naggert, H.; Kipgen, L.; Jasper-Toennies, T.; Rai, A.; Rudnik, J.; Nickel, F.; Arruda, L. M.; Bernien, M.; Kuch, W.; et al. Vacuum-Evaporable Spin-Crossover Complexes in Direct Contact with a Solid Surface: Bismuth versus Gold. *J. Phys. Chem. C* **2017**, *121* (2), 1210–1219.

(47) Bairagi, K.; Bellec, A.; Fourmental, C.; Iasco, O.; Lagoute, J.; Chacon, C.; Girard, Y.; Rousset, S.; Choueikani, F.; Otero, E.; et al. Temperature-, Light-, and Soft X-Ray-Induced Spin Crossover in a Single Layer of Fe^{II} -Pyrazolylborate Molecules in Direct Contact with Gold. *J. Phys. Chem. C* **2018**, *122* (1), 727–731.

(48) Kipgen, L.; Bernien, M.; Ossinger, S.; Nickel, F.; Britton, A. J.; Arruda, L. M.; Naggert, H.; Luo, C.; Lotze, C.; Ryll, H.; et al. Evolution of Cooperativity in the Spin Transition of an Iron(II) Complex on a Graphite Surface. *Nat. Commun.* **2018**, *9* (1), 2984.

(49) Wasinger E. C.; de Groot F. M. F.; Hedman B.; Hodgson K. O., Solomon E. I.. L-Edge X-

Ray Absorption Spectroscopy of Non-Heme Iron Sites: Experimental Determination of Differential Orbital Covalency. *J. Am. Chem. Soc.* **2003**, *125* (42), 12894-12906.

(50) Bonhommeau, S.; Ottosson, N.; Pokapanich, W.; Svensson, S.; Eberhardt, W.; Björneholm, O.; Aziz, E. F. Solvent Effect of Alcohols at the L-Edge of Iron in Solution: X-Ray Absorption and Multiplet Calculations. *J. Phys. Chem. B* **2008**, *112* (40), 12571–12574.

(51) Warland, A.; Antoniak, C.; Darbandi, M.; Weis, C.; Landers, J.; Keune, W.; Wende, H. Effect of Silica Capping on the Oxidation of Fe_3O_4 Nanoparticles in Dispersion Revealed by X-Ray Absorption Spectroscopy. *Phys. Rev. B* **2012**, *85* (23), 235113.

(52) Malavolti, L.; Lanzilotto, V.; Ninova, S.; Poggini, L.; Cimatti, I.; Cortigiani, B.; Margheriti, L.; Chiappe, D.; Otero, E.; Sainctavit, P.; et al. Magnetic Bistability in a Submonolayer of Sublimated Fe_4 Single-Molecule Magnets. *Nano Lett.* **2015**, *15* (1), 535–541.

(53) Kumar, S.; Prakash, R.; Choudhary, R. J.; Shukla, D. K.; Phase, D. M. Electronic Structure Studies of Fe Doped Eu_2O_3 Thin Film Using X-Ray Absorption and Resonant Photoemission Spectroscopy. *J. Alloys Compd.* **2017**, *711*, 598–602.

(54) van Schooneveld, M. M.; DeBeer, S. A Close Look at Dose: Toward L-Edge XAS Spectral Uniformity, Dose Quantification and Prediction of Metal Ion Photoreduction. *J. Electron Spectros. Relat. Phenomena* **2015**, *198*, 31–56.

(55) Pukenas, L.; Benn, F.; Lovell, E.; Santoro, A.; Kershaw Cook, L. J.; Halcrow, M. A.; Evans, S. D. Bead-like Structures and Self-Assembled Monolayers from 2,6-

Dipyrazolylpyridines and Their Iron(II) Complexes. *J. Mater. Chem. C* **2015**, *3* (30), 7890–7896.

SYNOPSIS. Two new heteroleptic complexes [Fe(1bppCOOH)(3bpp-bph)]$(ClO_4)_2$·solv (**1·solv**) and [Fe(1bppCOOH)(1bppCOOEt)]$(ClO_4)_2$·0.5Me_2CO (**2·0.5Me_2CO**) have been designed and prepared. The combination in **1** of 1bppCOOH and 3bpp-bph has resulted in an improvement of the SCO properties with respect to the homoleptic $[Fe(1bppCOOH)_2]^{2+}$ compound since a hysteretic thermal SCO closer to room temperature has been achieved. Besides, **2·0.5Me_2CO** represents the first heteroleptic complex based on two 1bpp type ligands, which stabilizes the LS state. Both compounds exhibit the LIESST effect.

Para ver esta película, debe
disponer de QuickTime™ y de
un descompresor .